Plug flow analysis for the design of the compaction region of a tapered screw extruder biomass briquetting machine

Ojolo S. J., Ajiboye, J. S., and Orisaleye, J. I.*

(Department of Mechanical Engineering, University of Lagos, Akoka, Lagos, Nigeria)

Abstract: The study of compaction or solids conveying in a screw extruder has been carried out majorly on the straight screws using the plug flow analysis. Despite this, the analysis of the straight screw appears to be complex as contained in existing literatures based on the force and torque balance. The tapered screw, which is considered to be an effective option for biomass compaction, introduces greater complications because the geometry is constantly changing. In this study, a method based on the traction and retardation mechanism of friction is developed for a fully unwound screw channel utilizing only the force balances. The procedure has been used to carry out a parametric analysis of the tapered screw extruder for a screw press biomass briquetting machine. The taper angle was considered to significantly increase the pressure developed in the extruder depending on the length of the compaction zone. The optimum taper angle has also been found to be dependent on the frictional coefficient of the biomass material with enclosing surfaces and ranges between 2° and 4°.

Keywords: plug flow analysis, biomass briquetting, tapered screw, extruder, friction

Citation: Ojolo, S. J., J. S. Ajiboye, and J. I. Orisaleye. 2015. Plug flow analysis for the design of the compaction region of a tapered screw extruder biomass briquetting machine. Agric Eng Int: CIGR Journal, 17(3): 176-195.

1 Introduction

The transport in a screw extruder results primarily from the differences in the friction and viscous forces at the contact locations screw-product and barrel-product. Weert et al. (2001) noted that the uniaxial compaction and single screw extrusion are closely related except that the helical screw configuration of the extruder is a much more complex geometry than the linear compaction cell. They also noted that another difference is that the wall friction in the extrusion process serves a dual purpose as traction and retarding mechanism. The plug flow theory has been used in the study of screw extruders (Darnell and Mol, 1956; Schneider, 1969; Tadmor and Klein, 1970; Lovegrove and Williams, 1970; Broyer and Tadmor, 1972; Campbell and Dontula, 1995; Weert et al., 2001). This study utilizes this theory in the study of compaction of bio-energetic materials particularly used in production of briquettes.

Several studies have been carried out on the uniaxial compaction of biomass materials for the production of briquettes. Although, several authors agree that the knowledge gained from uniaxial compaction is important to design efficient machines, the knowledge is yet to be translated into the design of the briquetting machines. It is important then that the knowledge available is applied to the design of the screw extruder for production of biomass briquettes. Tumuluru et al. (2010) have noted that the existing densification technologies available today have been developed for other enterprises and are not optimized for biomass-to-energy supply system logistics or a conversion facility's feedstock specification requirement. Hardman (2001) also stated that there is a need to describe and select the structural or geometric parameters of the screws scientifically noting that the existing method of screw selection has been largely on a trial-and-error basis. Gabrielle et al. (2001) had noted that extruders are adopted for a new use without preliminary design and

Received date: 2015-01-29 **Accepted date:** 2015-06-26
***Corresponding author: Orisaleye, J. I.,** Department of Mechanical Engineering, University of Lagos, Akoka, Lagos, Nigeria. Email: ifeorisaleye@gmail.com.

optimization in many cases. Practical problems which arise are mainly due to the difference in the rheological behavior of materials.

The compaction mechanism for densification of biomass has been described by different authors (Kaliyan and Morey, 2009; Mani et al., 2003; Tabil and Sokhansanj, 1996; Adapa et al., 2009). During the initial stages of compression, particles rearrange themselves under low pressure to form close packing and the air located in the interstices of the bulk material is removed. During this phase, the particles retain most of their properties, although energy is dissipated due to inter-particle and particle-to-wall friction. At high pressures, the particles are forced against each other and they undergo elastic and plastic deformation, thereby increasing inter-particle contact. As the particles approach each other, short range bonding forces become effective. At yield stress, brittle particles can fracture leading to the mechanical interlocking of particles. As pressure continues to increase, reduction in volume continues until the density of compacted material approaches true density of the particles. If the pressure applied is high enough to generate heat, then some components will locally melt. Once cooled, the molten material forms very strong solid bridges.

The focus of several of the existing studies on screw extrusion has been on the straight channel, constant pitch single screw extruder. According to Weert et al. (2001), the reason why the taper angle is often neglected is because many screws are straight. There are, however, other types of single screw extruders which have not been widely studied. These include the tapered screws, straight screws with varying pitch and tapered screws with a varying pitch. The use of the tapered screw appears to be an effective option for compaction in an extruder. According to Apruzzese (1998), the helix of the screw can be of constant pitch and depth from inlet to discharge but they are usually decreased to achieve complete barrel fill at the varying extrudate density. Matús et al. (2011) noted that the volume profile of one thread can be changed following the screw length by changing the outer diameter to form a conical screw, changing the profile depth to form a conical screw core, changing the pitch angle such that the screw has a progressive pitch.

It has been noticed from previous works that the compressibility of the material has not been included in the models. According to Weert et al. (2001), by maintaining a constant mass flow rate and allowing volumetric flow rate to vary with the density of the material, the compressibility of the material can be directly included in the model. Inclusion of compressibility in plug flow models assumes that the channel is filled at every section and at every instant during operation. Zhong (1991) noted that whilst the analysis of the straight screw appears to be complex as contained in existing literatures based on the force and torque balance, the tapered screw introduces greater complications because the geometry is constantly changing.

In this study, a simplified plug flow model developed for the straight screw is extended to determine the pressure distribution along the tapered screw extruder. The aim is to be able to select suitable parameters for the design of a tapered compaction zone of a screw extruder biomass briquetting machine and to investigate the effect of the design parameters on the operation of the screw extruder.

1.1 Biomass compaction models

The relationship between the pressure and density has been described by several researchers who have worked on different kinds of powdered and fibrous materials, including biomass. Experiments have been carried out by Kaminski (1989) and Pelt (2002) which have demonstrated that a power law empirical formula can be used to describe the densification process of different biomass materials. The empirical model is of the form $\rho = kP^n$. The power law coefficient, k, determines how tough a material is to compact with a smaller value of k requiring higher pressure to compact. The power law

index, n, characterizes the shape of the power curve with small values indicating that the density of the material increases slowly with increase in pressure.

Ennis et al. (2008) stated that the density of powders at an arbitrary pressure or stress σ, is given by a compaction equation of the form $\rho = \rho_o[\sigma/\sigma_o]^{1/m}$. They noted that ρ_o is the density at an arbitrary pressure or stress σ_o; ρ is the density at σ; and m is the compressibility of the powder. By comparing Ennis et al. (2008) with Kaminski (1989) and Pelt (2002), it is deduced that the power law index, n, is the inverse of the compressibility of the material. A similar equation in the form $\sigma/\sigma_o = A[\rho/\rho_o]^B$ was used by Matus et al. (2014) to describe the compressibility of the pine sawdust. The definitions of ρ_o, ρ, σ_o, σ are similar to Ennis et al. (2008). A is referred to as a constant regulating the form of the function and B is the coefficient of compressibility of particulate matter. B is similar to m when compared to Ennis et al. (2008). A number of compaction equations have developed over time for different materials. Table 1 presents a summary of some of the previous compaction equations and the materials they were used for (Adapa et al., 2009 and Mani et al., 2003).

Table 1 Compaction models for different materials

Compaction model	*Author*	*Material*
$\frac{V}{V_s} = c_1 \ln P + c_2$ $P = c_3\rho^{c_4}$	Walker (1923)	Non-metallic powders, sulphur, ammonium, sodium chloride and trinitrotoluene (Stewart, 1938) Adapa et al. (2002).
$\ln \rho = c_5 \ln P + c_6$	Jones (1960)	Metal powder
$\ln \frac{1}{1-\rho_f} = c_7 P + c_8$ $c_8 = \ln \frac{1}{1-\rho_o}$ $\rho_f = \frac{\rho}{\rho_1 x_1 + \rho_2 x_2}$	Heckel (1961)	Cellulose polymers (Shivanand and Sprockel, 1992) Food materials (Ollet et al., 1993)
$\frac{V_o - V}{V_o - V_s} = c_9 e^{-\frac{c_{10}}{P}} + c_{11} e^{-\frac{c_{12}}{P}}$	Cooper-Eaton (1962)	Alfalfa grinds
$\frac{PV_o}{V_o - V} = \frac{1}{c_{13}c_{14}} + \frac{P}{c_{15}}$	Kawakita and Ludde (1971)	Soft and fluffy powders.
$V = V_1 - c_{16} \log P + V_o \exp -\frac{P}{P_m}$	Sonnergaard (2001)	Pharmaceutical powders
$P = c_{17}\rho^{c_{18}}$ for $\rho < 400\ kg/m^3$ $P = c_{19} \ln \rho^{c_{20}}$ for $\rho > 400\ kg/m^3$	O'Dogherty and Wheeler (1984)	Fibrous straws
$\frac{\rho_{max} - \rho}{\rho_{max} - \rho_o} = e^{-\frac{\sigma}{K}}$	Bilanski et al. (1985)	Alfalfa and grass
$P = \frac{c_{21}\rho_o}{c_{22}} e^{\left(c_{23}\left(\left(\frac{\rho}{\rho_o}\right)-1\right)-1\right)}$	Faborode and O'Callaghan (1986)	Fibrous straws
$\rho = \rho_o + (c_{24} + c_{25}P)(1 - e^{-c_{28}P})$	Ferrero et al. (1991)	Straws
$P = c_{26} + c_{30}\rho + c_{31}\rho^2$	Viswanathan and Gothandapani (1999)	Coir pith

2 Model development

The compaction region of the screw extruder biomass briquetting machine is modelled using a plug flow analysis. The assumptions made in this analysis are similar to previous plug flow models (Darnel and Mol, 1956; Weert et al., 2001) with the exception that the screw is tapered and not straight which requires that the screw taper angle is taken into consideration. The assumptions are: the material flowing in the screw channel behaves as a solid plug and therefore there is no internal shearing; screw is filled with material, therefore interface contact occurs between the plug and confining geometry; Coulomb frictional conditions exist at the contact interface between the material and metal with the friction coefficient at the screw different from that at the

barrel; the coefficients of friction acting at contact surfaces are independent of pressure and temperature; effects of gravity and the centripetal and Coriolis acceleration are neglected; pressures developed within the plug are non-isotropic with the pressures developed in the lateral directions having values lower than the applied pressure in the longitudinal direction.

2.1 Basic geometry of a straight and tapered screw extruder

(a) Straight screw

The basic geometry of the single screws used in extruders and the relationships between the terms identified in the geometry of the single screw extruder shown in Figure 1.

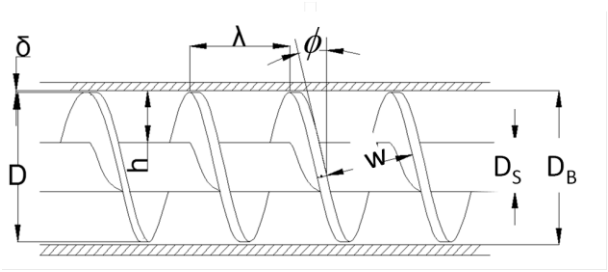

Figure 1 The basic geometry of a straight single screw extruder

The relationship between the root diameter of the screw, D_S, and the internal diameter of the barrel, D_B, is as Equation 1:

$$D_B = D_S + 2h \quad (1)$$

Considering the clearance, δ, between the screw flight and the barrel, the screw flight diameter, D, is estimated as Equation 2:

$$D = D_B - 2\delta = D_S + 2(h - \delta) \quad (2)$$

The axial distance associated with one full turn of the screw flight is the screw pitch, or lead, assuming a thread with single flight. Considering Figure 2, which shows the unwound screw channel in one revolution to form a straight channel, the screw pitch, λ, is related to the mean diameter of screw flight, D, and helix angle, ϕ, by Equation 3:

$$\lambda = \pi D \tan\phi \quad (3)$$

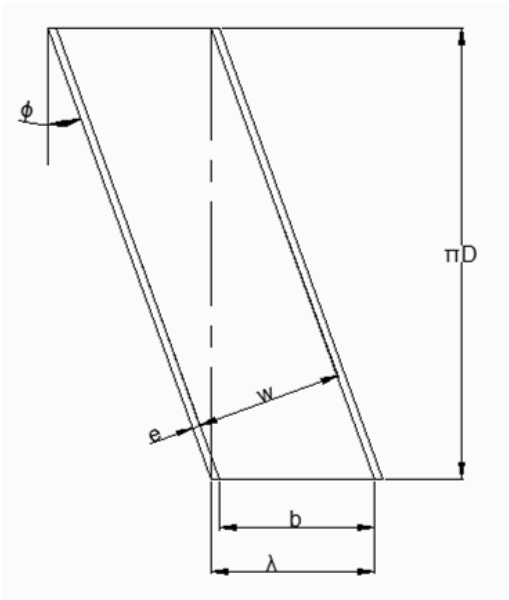

Figure 2 Developed screw channel of the single screw extruder

From Figure 2, it is possible to establish a relationship between the axial distance between flights, b, flight thickness, e, and the screw pitch, λ, which is given as Equation 4:

$$\lambda = b + \frac{e}{\cos\phi} \quad (4)$$

The axial distance between flights, b, and the perpendicular distance between flights, w, is related by the expression as Equation 5:

$$w = b\cos\phi \quad (5)$$

Hence, combining Equation 4 and Equation 5 would give Equation 6:

$$w = \lambda\cos\phi - e \quad (6)$$

By combining Equation 2 and Equation 3 with Equation 6, see Equation 7:

$$w = \pi(D_B - 2\delta)\sin\phi - e \quad (7)$$

Alternatively, Equation 7 can be written in terms of the screw root diameter, D, and the channel depth, h, as Equation 8:

$$w = \pi[D_S + 2(h - \delta)]\sin\phi - e \quad (8)$$

Equation 7 and Equation 8 represent the perpendicular distance between flights which is also the

width of the channel when the screw flight is unwound into a straight channel.

(b) Tapered screw

This section presents the variation in geometry of the tapered screw compared to straight screw. Figure 3 shows an illustration of the tapered screw and its geometry. The taper angle of the channel is θ while the taper angle of the screw is ϑ. The smallest depth of the channel, h, is the depth at the end of the compression region.

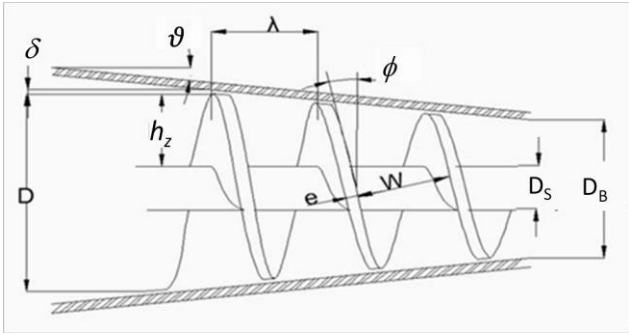

Figure 3 Geometry of the tapered single screw extruder

From the geometry, it can be observed that the channel depth is a function of the channel length. Hence, the channel depth at any section along the screw channel is estimated using Equation 9:

$$h_z = h + Z\tan\theta \quad (9)$$

Since the channel depth varies with channel length, the screw diameter and consequently, the barrel diameter, also vary with the channel depth. The barrel diameter, a function of channel length, at any section is as Equation 10:

$$D_B = D_S + 2h_z \quad (10)$$

Alternatively, the barrel diameter is as Equation 11:

$$D_B = D_S + 2(h + Z\tan\theta) \quad (11)$$

With consideration of the clearance, the screw diameter at any section, Z, along the channel length can be written as Equation 12:

$$D = D_B - 2\delta = D_S + 2(h + Z\tan\theta - \delta) \quad (12)$$

2.2 Traction and retardation mechanism

The mechanism used in the development of the models considers two extremes of the relative motions between the plug, screw and barrel. In the first instance, the barrel is stationary, the plug sticks to the barrel and the screw is allowed to move in such a way that the plug is transported forward in the screw channel. This is similar to what will happen when the barrel and plug move together within a stationary screw channel in such a way that the plug is transported in the same direction. In the next instance, the barrel is held stationary but the plug slips on the barrel and sticks to the screw. The screw is allowed to move relative to the barrel carrying the plug in a direction such that it moves forward within the screw channel. Again, this is similar to what happens when the screw and plug are stationary and the barrel slides in such a way that the plug moves in the forward direction. This mechanism is used to determine the direction of frictional forces acting on the plug. An elemental slice of the plug flowing in the channel is analysed by carrying out a force balance on it. The element and forces acting on it are shown in Figure 4.

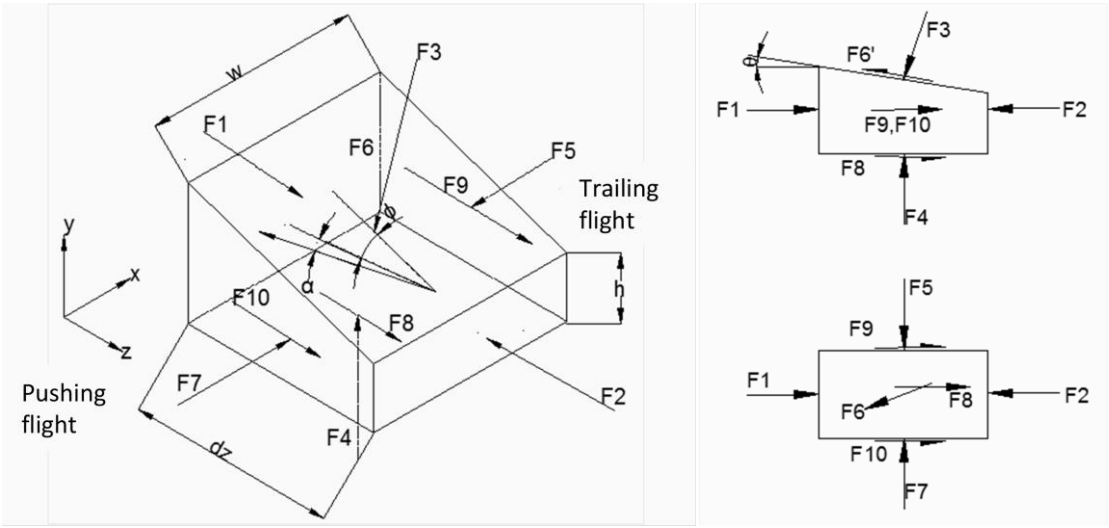

Figure 4 Forces acting on elemental slice of plug in inclined channel (front and plan views)

From Figure 4, $F8$, $F9$ and $F10$ are frictional forces on the screw. The force $F6$ occurs at the barrel surface. The force $F1$ is greater than $F2$ by an amount caused by a differential pressure which causes the plug to move in the channel. From the figure, it seems that the friction at the barrel is the retarding force and those at the screw are the traction forces. Contrarily, Rauwendaal (2004) explained that if the screw was to rotate with the material in the channel without friction at the barrel, there would be no forward movement of the material. The friction at the barrel is, therefore, considered to produce the traction effect since it is responsible for the forward movement of the material.

2.3 Pressure development in the screw extruder

The pressure developed in the plug is assumed to be non-isotropic with the pressure in the down-channel or longitudinal direction taken as the driving pressure, the relationship of pressures in other lateral directions is given as Equation 13:

$$P_x = P_y = \kappa P_z = \kappa P \tag{13}$$

The term κ is the stress transmission coefficient or Janseen coefficient which gives the relationship between the applied pressure and the lateral pressure and is estimated by Equation 14(Ennis et al., 2008):

$$\kappa = \frac{1 - \sin\psi_e}{1 + \sin\psi_e} \tag{14}$$

The parameter, ψ_e, is the effective angle of powder friction with typical values ranging from 40 ° to 60 °. For the slice of plug shown in Figure 4, it is considered that the slice is sufficiently thin such that the height of the element at the flow area of the face up-channel where force F1 acts, is the same as the height of the flow area of the face down-channel where force F2 acts. The average height is, therefore, used such that Equation 15

$$\bar{h} = h + \frac{dz}{2}\tan\theta \tag{15}$$

Therefore, the forces acting on the slice in the down-channel, or z-direction, $F1$ and $F2$ are as Equation 16 and Equation 17:

$$F1 = (P + dP)\left(h + \frac{dz}{2}\tan\theta\right)w \tag{16}$$

$$F2 = Pw\left(h + \frac{dz}{2}\tan\theta\right) \tag{17}$$

The force, $F4$, produced from the lateral pressure acting at the bottom of the plug is due to stress, or pressure, transmission, is as Equation 18

$$F4 = \kappa P w\, dz \tag{18}$$

The frictional force, $F8$, due to the pressure acting at the bottom of the slice is as Equation 19

$$F8 = \mu_S F4 = \mu_S \kappa P w\, dz \tag{19}$$

The force, $F5$, from the lateral pressure on the trailing flight is due to stress, or pressure transmission, and is as Equation 20

$$F5 = \kappa P\, dz\left(h + \frac{dz}{2}\tan\theta\right) \tag{20}$$

The frictional force, $F9$, acting on the trailing face due to the lateral pressure acting on the face is as Equation 21

$$F9 = \mu_f F5 = \mu_f \kappa P\, dz\left(h + \frac{dz}{2}\tan\theta\right) \tag{21}$$

By taking a force balance in the y-direction, see Equation 22

$$F4 = F3\cos\theta - F6\cos(\phi + \alpha)\sin\theta \tag{22}$$

From the diagram, it can be observed that $F6$ is the frictional force at the material-barrel interface and is related to $F3$ by Equation 23:

$$F6 = \mu_B F3 \tag{23}$$

Therefore, Equation 18 and Equation 23 can be substituted into Equation 22 such that it becomes Equation 24:

$$\kappa P w\, dz = F3\cos\theta - \mu_B F3\cos(\phi + \alpha)\sin\theta \tag{24}$$

The force acting at the barrel surface, $F3$, can then be determined as :

$$F3 = \frac{\kappa P w\, dz}{\cos\theta - \mu_B\cos(\phi + \alpha)\sin\theta} \tag{25}$$

The frictional force acting at the material-barrel interface can therefore be determined as Equation 26:

$$F6 = \frac{\mu_B \kappa P w\, dz}{\cos\theta - \mu_B\cos(\phi + \alpha)\sin\theta} \tag{26}$$

It is seen that the forces acting at the barrel surface of the tapered screw extruder is affected by the taper angle, the screw geometry and the frictional coefficient. These also affect the forces on the pushing flight since it must overcome the friction generated at the material-barrel interface.

Taking a force balance in the lateral x-direction, as Equation 27

$$F7 = F5 + F6\cos\theta\sin(\phi + \alpha) \tag{27}$$

By substituting Equation 20 and Equation 26 into Equation 27 such as to replace $F5$ and $F6$ respectively, the force on the pushing flight is obtained as Equation 28:

$$F7 = \kappa P\, dz\left(h + \frac{dz}{2}\tan\theta\right) + \frac{\mu_B \kappa P w\, dz\cos\theta\sin(\phi + \alpha)}{\cos\theta - \mu_B\cos(\phi + \alpha)\sin\theta} \tag{28}$$

The frictional force, $F10$, on the pushing flight resulting from the pressure transmission together with the force required to overcome friction at the barrel is as Equation 29:

$$F10 = \mu_f\left[\kappa P\, dz\left(h + \frac{dz}{2}\tan\theta\right) + \frac{\mu_B \kappa P w\, dz\cos\theta\sin(\phi + \alpha)}{\cos\theta - \mu_B\cos(\phi + \alpha)\sin\theta}\right] \tag{29}$$

A force balance can be taken in the down-channel, or z-direction such that Equation 30:

$$F1 = F2 + F3\sin\theta + F6\cos(\phi + \alpha)\cos\theta - F8 - F9 - F10 \tag{30}$$

By substituting the forces with equations derived for them from Equation 16 to Equation 29 and simplifying, Equation 30 becomes Equation 31:

$$\frac{dP}{P} = \frac{\kappa\, dz}{h[1 - \mu_B\cos(\phi + \alpha)\tan\theta]}\left\{\mu_B\cos(\phi + \alpha) - \mu_S\left(1 + 2\frac{\mu_f}{\mu_S}\frac{h}{w}\right) - \mu_f\mu_B\sin(\phi + \alpha) + \tan\theta\left[1 + \mu_S\mu_B\left(1 + 2\frac{\mu_f}{\mu_S}\frac{h}{w}\right)\cos(\phi + \alpha)\right]\right\} \tag{31}$$

By integrating Equation (31) taking an initial condition from $P(0) = P_o$, the pressure along the length of the channel is as Equation 32:

$$\ln\frac{P_z}{P_o}=\frac{\kappa Z}{h[1-\mu_B\cos(\phi+\alpha)\tan\theta]}\left\{\mu_B\cos(\phi+\alpha)-\mu_S\left(1+2\frac{\mu_f}{\mu_S}\frac{h}{w}\right)-\mu_f\mu_B\sin(\phi+\alpha)+\tan\theta\left[1+\mu_S\mu_B\left(1+2\frac{\mu_f}{\mu_S}\frac{h}{w}\right)\cos(\phi+\alpha)\right]\right\} \quad (32)$$

The channel taper angle is different from the screw taper angle and a relationship can be obtained for the two angles. The channel taper angle is obtained from the change in channel depth along the length of the channel as Equation 33:

$$\tan\theta=\frac{D_1-D_2}{2Z} \quad (33)$$

Similarly, the screw taper angle is obtained from the change in channel depth along the length of the screw as Equation 34

$$\tan\vartheta=\frac{D_1-D_2}{2Z_S} \quad (34)$$

The relationship between the length of the channel and axial length of the screw is as Equation 35:

$$Z_S=Z\sin\phi \quad (35)$$

By combining Equation 33, Equation 34 and Equation 35, the relationship between the screw taper angle and the channel taper angle is as Equation 36:

$$\tan\theta=\tan\vartheta\sin\phi \quad (36)$$

By substituting Equation 35 and Equation 36 into Equation 32, the pressure developed along axial length of the screw is as Equation 37:

$$\ln\frac{P_z}{P_o}=\frac{\kappa Z_S}{h\sin\phi\,[1-\mu_B\cos(\phi+\alpha)\tan\vartheta\sin\phi]}\left\{\mu_B\cos(\phi+\alpha)-\mu_S\left(1+2\frac{\mu_f}{\mu_S}\frac{h}{w}\right)-\mu_f\mu_B\sin(\phi+\alpha)+\tan\vartheta\sin\phi\left[1+\mu_S\mu_B\left(1+2\frac{\mu_f}{\mu_S}\frac{h}{w}\right)\cos(\phi+\alpha)\right]\right\} \quad (37)$$

For a pressure at the end of the compaction region taken as P_{max}, the length of the tapered screw required to achieve compaction is obtained from Equation 37 as Equation 38:

$$L_S=\frac{h\sin\phi\,[1-\mu_B\cos(\phi+\alpha)\tan\vartheta\sin\phi]}{\kappa\left\{\begin{array}{l}\mu_B\cos(\phi+\alpha)-\mu_S\left(1+2\frac{\mu_f}{\mu_S}\frac{h}{w}\right)-\mu_f\mu_B\sin(\phi+\alpha)\\ +\tan\vartheta\sin\phi\left[1+\mu_S\mu_B\left(1+2\frac{\mu_f}{\mu_S}\frac{h}{w}\right)\cos(\phi+\alpha)\right]\end{array}\right\}}\cdot\ln\frac{P_{max}}{P_o} \quad (38)$$

The estimated screw length is the lower limit of the projected length of the screw extruder.

2.4 Volumetric flow rate of the straight screw extruder

Ennis et al. (2008) noted that the flow in the compaction region of the screw extruder is a drag induced flow. Zhong (1991) also stated that the maximum flow rate in the extruder channel equals the drag flow. To determine the velocity of the plug flowing through the channel of the tapered screw extruder, Figure 5 is considered. Figure 5(a) shows the velocity diagram while Figure 5(b) shows the relationship between velocities at the plug surface and barrel surface on a plane drawn through V_b. V_{ps} is the velocity of the plug along the axial length of the screw, V_b is the velocity of the plug surface in contact with the barrel, V_p is the velocity of the plug along the channel, and V_{bp} is the relative velocity of the plug relative to the barrel. By resolving the velocities on the inclined plane, it can be deduced that the barrel velocity is as Equation 39:

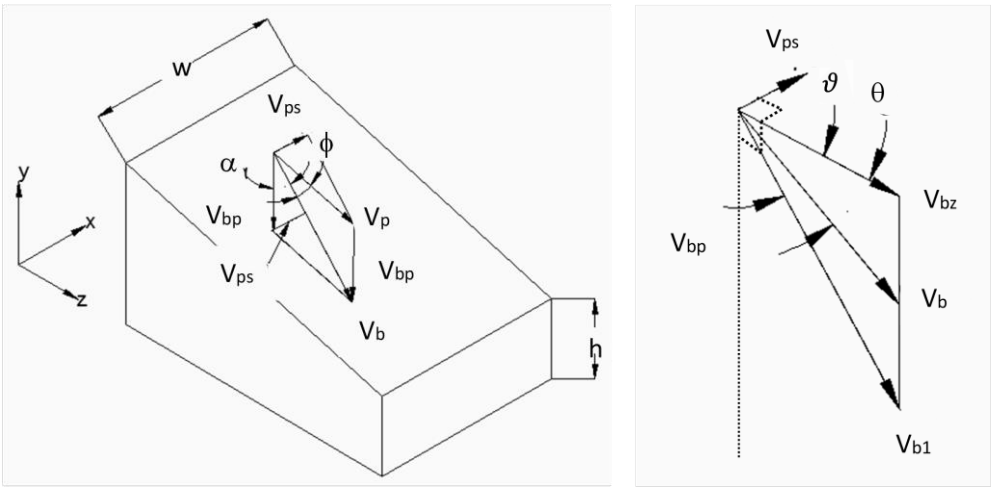

Figure 5(a) Velocities of the plug flowing through a tapered screw extruder channel; (b) relationship between velocities of on surfaces of plug and barrel

$$V_b = \frac{V_{ps}}{\tan\alpha} + \frac{V_{ps}}{\tan\phi} \tag{39}$$

Therefore, the velocity of the plug along the screw axis is as Equation 40:

$$V_{ps} = \frac{V_b \tan\alpha \tan\phi}{\tan\alpha + \tan\phi} \tag{40}$$

The velocity of the plug along the channel is obtained from the sine rule, see Equation 41

$$\frac{V_p}{\sin\alpha} = \frac{V_{bp}}{\sin\phi} \tag{41}$$

Therefore, Equation 42

$$V_p = \frac{V_{bp} \sin\alpha}{\sin\phi} \tag{42}$$

But, the plug velocity along the screw axis is related to the relative velocity between the barrel and plug by Equation 43:

$$V_{ps} = V_{bp} \sin\alpha \tag{43}$$

By combining Equation 40, Equation 42 and Equation 43, the velocity of the plug along the screw channel is as Equation 44:

$$V_p = \frac{V_b \tan\alpha \sec\phi}{(\tan\alpha + \tan\phi)} \tag{44}$$

The axial plug velocity required to compute the flow rate through the channel is the velocity of the plug parallel to the unwound screw root of the channel. This is obtained by resolving V_p to give Equation 45:

$$V_{pz} = \frac{V_b \cos\theta \tan\alpha \sec\phi}{(\tan\alpha + \tan\phi)} \tag{45}$$

Figure 5(b), however, shows that there is a distinction between the velocities, V_b, measured at the surface of the plug, and the actual velocity of the screw at the barrel V_{b1}. This is due to the distinction between the screw channel taper angle and the screw taper angle. The two are related to the axial velocity of the plug in the channel as Equation 46:

$$V_{bz} = V_b \cos\theta = V_{b1} \cos\vartheta \tag{46}$$

The velocity of the screw at the barrel is as Equation 47:

$$V_{b1} = \pi[D_S + 2(h + Z_s \tan\vartheta)]N \tag{47}$$

Therefore, Equation (45) can be written as Equation 48:

$$V_{pz} = \frac{\pi[D_S + 2(h + Z_s \tan\vartheta)]N \cos\vartheta \tan\alpha \sec\phi}{(\tan\alpha + \tan\phi)} \tag{48}$$

Due to the changing diameter of the screw, and consequently the barrel, the equation for the channel area along the length of the channel is as Equation 49:

$$A = wh = \pi[D_S + 2(h + Z_s \tan\vartheta - \delta)]h \sin\phi \left[1 - \frac{e}{\pi[D_S + 2(h + Z_s \tan\vartheta - \delta)]\sin\phi}\right] \quad (49)$$

By taking the entry as the reference point, the volumetric throughput, being the product of the channel area and the axial velocity of flow through the channel is as Equation 50:

$$Q = \pi^2[D_S + 2(h + \langle L_S - Z_S\rangle \tan\vartheta - \delta)][D_S + 2(h + \langle L_S - Z_S\rangle \tan\vartheta)]Nh\frac{\cos\vartheta \tan\alpha \tan\phi}{(\tan\alpha + \tan\phi)}\left[1 - \frac{e}{\pi[D_S + 2(h + \langle L_S - Z_S\rangle \tan\vartheta - \delta)]\sin\phi}\right] \quad (50)$$

To obtain the mass throughput, the volumetric throughput is multiplied by the density. Since the screw dimensions are changing, it is expected that the density of the material being processed changes in like manner with the screw. Based on the assumption that the screw is always filled, the density change must therefore match the volume change of screw which will require that the mass flow rate should be constant.

2.5 Variation of density with pressure in a tapered screw extruder

Using compaction equation presented by Ennis et al. (2008) together with the pressure developed in of the compaction region in Equation 37, the variation of density along the axis of the tapered screw from the entry towards the exit can be determined as Equation 51:

$$\rho = \rho_o \exp\left[\frac{1}{m}\left[\left[\frac{\kappa Z_S}{h\sin\phi\,[1-\mu_B\cos(\phi+\alpha)\tan\vartheta\sin\phi]}\left\{\mu_B\cos(\phi+\alpha)\right.\right.\right.\right.$$
$$-\mu_S\left(1+2\frac{\mu_f}{\mu_S}\frac{h}{w}\right)-\mu_f\mu_B\sin(\phi+\alpha)$$
$$\left.\left.\left.\left.+\tan\vartheta\sin\phi\left[1+\mu_S\mu_B\left(1+2\frac{\mu_f}{\mu_S}\frac{h}{w}\right)\cos(\phi+\alpha)\right]\right\}\right]\right]\right] \quad (51)$$

If a backward modelling of the screw extruder is considered, the equation takes the form Equation 52:

$$\rho = \rho_{max} \exp\left[\frac{1}{m}\left[\left[\frac{\kappa(Z_S-L_s)}{h\sin\phi\,[1-\mu_B\cos(\phi+\alpha)\tan\vartheta\sin\phi]}\left\{\mu_B\cos(\phi+\alpha)\right.\right.\right.\right.$$
$$-\mu_S\left(1+2\frac{\mu_f}{\mu_S}\frac{h}{w}\right)-\mu_f\mu_B\sin(\phi+\alpha)$$
$$\left.\left.\left.\left.+\tan\vartheta\sin\phi\left[1+\mu_S\mu_B\left(1+2\frac{\mu_f}{\mu_S}\frac{h}{w}\right)\cos(\phi+\alpha)\right]\right\}\right]\right]\right] \quad (52)$$

ρ_o and ρ_{max} are the densities at the entry and exit regions of the compaction zone respectively and they correspond to pressures P_o and P_{max} respectively.

2.6 Mass throughput and compaction ratio of a tapered screw extruder

The mass throughput has been defined as the product of the density and the volumetric flow rate at any section. The mass flow rate at the exit of the compaction region, $Z_s = L_s$, is given as Equation 53:

$$\dot{m} = \pi^2\rho_{max}[D_S+2(h-\delta)][D_S+2h]Nh\frac{\cos\vartheta\tan\alpha\tan\phi}{(\tan\alpha+\tan\phi)}\left[1\right.$$
$$\left.-\frac{e}{\pi[D_S+2(h-\delta)]\sin\phi}\right] \quad (53)$$

The mass throughput at any section along the screw can be written by combining Equation 52, which is the density distribution along the screw axis, with Equation 50, which represents the drag flow along the axis, such that Equation 54:

$$\dot{m} = \pi^2\rho_{max}[D_S+2(h+\langle L_S-Z_S\rangle\tan\vartheta-\delta)][D_S+2(h$$
$$+\langle L_S-Z_S\rangle\tan\vartheta)]Nh\frac{\cos\vartheta\tan\alpha\tan\phi}{(\tan\alpha+\tan\phi)}\left[1\right.$$
$$\left.-\frac{e}{\pi[D_S+2(h+\langle L_S-Z_S\rangle\tan\vartheta-\delta)]\sin\phi}\right]$$
$$\cdot\exp\left[\frac{1}{m}\left[\left[\frac{\kappa(Z_S-L_s)}{h\sin\phi\,[1-\mu_B\cos(\phi+\alpha)\tan\vartheta\sin\phi]}\left\{\mu_B\cos(\phi+\alpha)\right.\right.\right.\right.$$
$$-\mu_S\left(1+2\frac{\mu_f}{\mu_S}\frac{h}{w}\right)-\mu_f\mu_B\sin(\phi+\alpha)$$
$$\left.\left.\left.\left.+\tan\vartheta\sin\phi\left[1+\mu_S\mu_B\left(1+2\frac{\mu_f}{\mu_S}\frac{h}{w}\right)\cos(\phi+\alpha)\right]\right\}\right]\right]\right] \quad (54)$$

$$\dot{m} = \pi^2 \rho_{max}[D_S + 2(h + L_S \tan\vartheta - \delta)][D_S + 2(h + L_S \tan\vartheta)]Nh \frac{\cos\vartheta \tan\alpha \tan\phi}{(\tan\alpha + \tan\phi)} \left[1 - \frac{e}{\pi[D_S + 2(h + L_S \tan\vartheta - \delta)]\sin\phi}\right] \cdot \exp\left[\frac{1}{m}\left[\frac{-\kappa L_S}{h \sin\phi\,[1 - \mu_B \cos(\phi + \alpha)\tan\vartheta \sin\phi]}\left\{\mu_B \cos(\phi + \alpha) - \mu_S\left(1 + 2\frac{\mu_f}{\mu_S}\frac{h}{w}\right) - \mu_f \mu_B \sin(\phi + \alpha) + \tan\vartheta \sin\phi\left[1 + \mu_S \mu_B\left(1 + 2\frac{\mu_f}{\mu_S}\frac{h}{w}\right)\cos(\phi + \alpha)\right]\right\}\right]\right] \quad (55)$$

If the mass flow rate is held constant at any given section of the screw and the volumetric flow rate is allowed to vary with the density of the material, Equation 53 and Equation 55 can then be combined using a continuity equation. The resulting equation is used to determine the compaction ratio of the screw extruder and is stated in Equation 56.

$$\exp\left[\frac{1}{m}\left[\frac{\kappa L_S}{h \sin\phi\,[1 - \mu_B \cos(\phi + \alpha)\tan\vartheta \sin\phi]}\left\{\mu_B \cos(\phi + \alpha) - \mu_S\left(1 + 2\frac{\mu_f}{\mu_S}\frac{h}{w}\right) - \mu_f \mu_B \sin(\phi + \alpha) + \tan\vartheta \sin\phi\left[1 + \mu_S \mu_B\left(1 + 2\frac{\mu_f}{\mu_S}\frac{h}{w}\right)\cos(\phi + \alpha)\right]\right\}\right]\right] = [D_S + 2(h + L_S \tan\vartheta - \delta)][D_S + 2(h + L_S \tan\vartheta)]Nh \frac{\cos\vartheta \tan\alpha \tan\phi}{(\tan\alpha + \tan\phi)} \cdot \frac{\left[1 - \frac{e}{\pi[D_S + 2(h + L_S \tan\vartheta - \delta)]\sin\phi}\right]}{[D_S + 2(h - \delta)][D_S + 2h]Nh \frac{\cos\vartheta \tan\alpha \tan\phi}{(\tan\alpha + \tan\phi)}\left[1 - \frac{e}{\pi[D_S + 2(h - \delta)]\sin\phi}\right]} \quad (56)$$

Each term on either side of the equality sign represents the compaction ratio. The compaction ratio based on density change is the expression on the left hand side of the equation given as Equation 57:

$$\gamma_\rho = \exp\left[\frac{1}{m}\left[\frac{\kappa L_S}{h \sin\phi\,[1 - \mu_B \cos(\phi + \alpha)\tan\vartheta \sin\phi]}\left\{\mu_B \cos(\phi + \alpha) - \mu_S\left(1 + 2\frac{\mu_f}{\mu_S}\frac{h}{w}\right) - \mu_f \mu_B \sin(\phi + \alpha) + \tan\vartheta \sin\phi\left[1 + \mu_S \mu_B\left(1 + 2\frac{\mu_f}{\mu_S}\frac{h}{w}\right)\cos(\phi + \alpha)\right]\right\}\right]\right] \quad (57)$$

The compaction ratio based on the change in volume of the screw channel is the right hand side of the equation given as Equation 58:

The taper angle at which the compaction ratio based on the change in the volume of screw channel corresponds with the compaction ratio based on change in density will give the optimum taper angle.

3 Discussions

3.1 Discussion of models

The models developed for the pressure build-up in the tapered compaction zone of a screw extruder are found to be consistent with the exponential forms described in previous works and reports carried out on the compaction zone of the straight screw extruder (Matus et al., 2011; Weert et al., 2001; Broyer and Tadmor, 1972). The general representation being of the form Equation 59:

$$P = P_o e^{\frac{\mu_* z}{h}} \tag{59}$$

As reported earlier, past plug flow models utilized force and torque balances which appeared to be complex and the inclusion of the screw taper into the analysis increases the level of complications (Zhong, 1991). In this study, based on the understanding of the traction and retardation based mechanism of friction, the approach to the model for the tapered screw is much simplified. The equations obtained can be checked with previous models for the straight screw extruder by comparing the overall friction coefficient, μ_*. The overall friction coefficient for the tapered screw in the present work is as Equation 60

$$\begin{aligned}\frac{1}{[1-\mu_B\cos(\phi+\alpha)\tan\vartheta\sin\phi]}\Big\{&\mu_B\cos(\phi\\&+\alpha)-\mu_S\left(1+2\frac{\mu_f}{\mu_S}\frac{h}{w}\right)\\&-\mu_f\mu_B\sin(\phi+\alpha)\\&+\tan\vartheta\sin\phi\Big[1\\&+\mu_S\mu_B\Big(1\\&+2\frac{\mu_f}{\mu_S}\frac{h}{w}\Big)\cos(\phi+\alpha)\Big]\Big\}\end{aligned} \tag{60}$$

If the taper angle is neglected, and the friction coefficients μ_f and μ_S are equal, equation (60) becomes similar to the overall friction coefficient reported by Weert et al. (2001) for a simplified Darnel and Mol (1956) model for unwound geometry stated as Equation 61:

$$\begin{aligned}\mu_* = \mu_B\cos(\phi+\alpha)-(1+2\beta)\mu_S\\-\mu_B\mu_S\sin(\alpha+\phi)\end{aligned} \tag{61}$$

In addition to the simplifications, the original Darnel and Mol model also assumed hydrostatic stress, $\kappa = 1$, which has been widely refuted in subsequent works. The present study utilized a stress transmission coefficient, although Weert et al. (2001) utilized a parameter which is a function of the Poisson ratio of the material.

For the model in Equation 37, the initial pressure is taken as the pressure at the bottom of the hopper. Tadmor and Klein (1970) and Agur (1982) have reported suitable equations for the determination of this pressure. Equation 38 gives the required compaction length of the screw having predetermined other parameters. The required compaction length of the screw is the minimum length of the screw for the extruder.

Equation 51 shows how the density will vary with from the beginning of the compaction zone to the end of the compaction zone while Equation 52 shows how the density will vary in the reversed direction. As can be seen, the density, being related to the pressure will vary exponentially with the length of the extruder. The compaction ratios have been obtained by allowing the density and volume flow of the screw change while holding the mass flow rate through every section constant, particularly the inlet and exit sections of the compaction zone. The compaction ratio based on the change in density must therefore match the compaction ratio based on the change in volume. Hence, by plotting both ratios on a graph, the optimum compaction ratio can be obtained.

3.2 Simulation parameters

The parameters used in the simulation of the compaction region are stated in Table 2. The maximum compaction pressure, or working pressure, required at

the end of the compaction zone is assumed to be 100 MPa and the pressure at the bottom of the hopper which is also the pressure at the start of the compaction is 0.2 MPa. From the study carried out by Larsson (2010), kinetic friction coefficient ranges between 0.1 and 0.6 depending on the normal stress and moisture content. Sitkei (1986) also stated that the dynamic friction coefficient of biomass material on steel is 0.35. Ennis et al. (2008) stated that the effective angle of powder friction ranges between 45 ° and 60 ° but Zhong (1991) argued that it was 76 close to the angle of repose of the material. For this study a screw speed between 100 to 150 rpm is considered. The solids conveying angle is less than 5 ° in most applications of the screw extruder usually in the range of 2 °to 3 °(Weert, 2001).

Table 2 Parameters utilized in the simulation of the compaction zone of the screw extruder biomass briquetting machine

Parameter	Value
Compacting Pressure, P_{max}	100 MPa
Friction coefficient, μ_B or μ_S	0.1-0.6
Channel Depth, h	20 mm
Screw root diameter, D_S	30 mm
Effective angle of powder friction, ψ_e	45°
Flight thickness, e	5 mm
Screw Speed, N	100-150 r/min
Solids conveying angle, α	2°

3.3 Pressure development in the tapered compaction region of the screw extruder

a Effect of friction coefficients of biomass material on barrel and screw

The effect of friction coefficient between the material of the biomass and the barrel, μ_B is shown in Figure 6(a). It is seen that the pressure develops quickly with a higher friction coefficient at the barrel. As can be deduced from Figure 6(b), a shorter length of the compaction zone will be required for a higher frictional coefficient between the biomass material and the barrel.

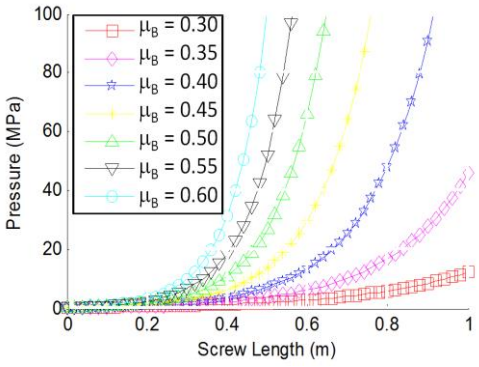

（a）

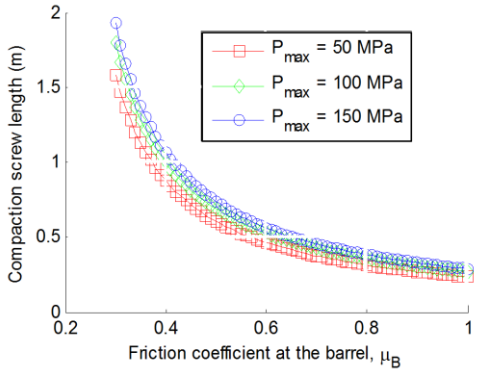

(b)

Figure 6 Effect of the friction coefficient between biomass and barrel on (a) pressure developed in the compaction zone; (b) length of compaction zone

For the friction coefficient at the screw, μ_S, however, the pressure developed in the compaction zone reduces with an increase in the friction coefficient. This is shown in Figure 7(a). Figure 7(b) shows how the required compaction length will vary with the friction coefficient of the screw. It is seen that as the friction coefficient increases, a longer compaction zone will be required to develop a specified pressure.

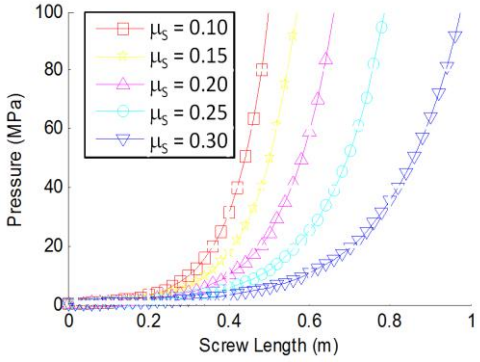

(a)

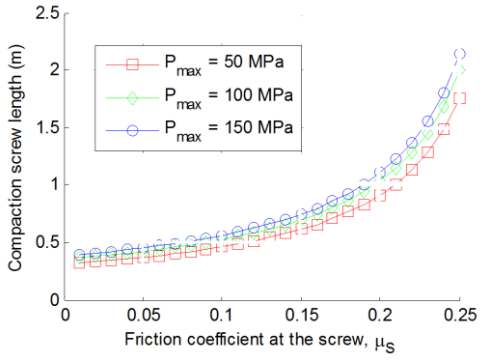

(b)

Figure 7 Effect of friction coefficient between biomass and screw on (a) pressure developed in the compaction zone; (b) length of compaction zone

b Effect of screw taper angle

The effect of the screw taper on the pressure developed in the compaction region of the screw extruder is shown in Figure 8. It is seen that the effect of the taper angle of the screw becomes much significant as the length of the compaction zone increases. For a screw compaction length of 50 cm, it is seen that the pressure is about 60 MPa with the given parameters for a straight screw but with a screw taper angle of 4°, the pressure is about 90 MPa. As such, the taper angle may not be neglected in plug flow models due to this significance. However, there should be an optimum taper angle for the smooth operation of the extruder depending on the properties of material being extruded.

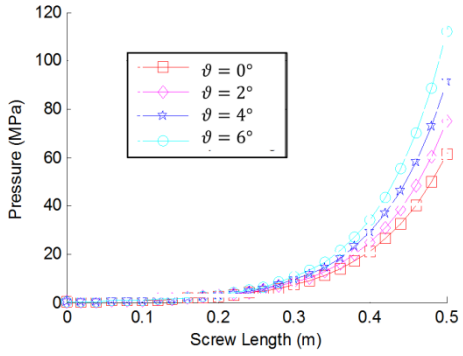

Figure 8 Effect of taper angle of the screw on the pressure build-up in the compaction zone of a screw extruder biomass briquetting machine

3.4 Optimum taper angle for the screw extruder briquetting machine

The optimum taper angle for the compaction zone of the screw extruder can be determined by examining together the effect of the variation of density along the extruder with the variation of volumetric throughput along the section of the extruder. The compaction ratio based on density change has been derived in Equation 57 while Equation 58 shows the compaction ratio based on volume change of screw channel. The optimum taper angle is the taper angle at which the change in volume of screw flight corresponds to the density variation of the biomass material. This was determined by holding the mass rate constant and allowing the volumetric flow rate vary with density of the biomass material along the length of the screw extruder.

Information on the coefficient of compressibility obtained from different researchers during compaction of some biomass materials is presented in Table 3. It is seen from Matus et al. (2014) that the particle size affects the coefficient of compressibility but it is also known that in practical production of briquettes, the particle sizes are not uniform but distributed. Hence, ranges of coefficient of compressibility should be between 3.0 and 4.5 to cover a wide range of biomass materials. Pelt (2003) had noted that the n-values, which are the reciprocals of the coefficient of compressibility, are consistent with the general value proposed by Kaminski et al. (1989).

Table 3 Coefficient of compressibility of some biomass materials

Biomass Material	Coefficient of Compressibility		Source
	n	$m = 1/n$	
Pine Sawdust (0.0 – 0.5 mm)	0.13*	7.97	Matus et al. (2014)
Pine Sawdust (0.5 – 1.0 mm)	0.14*	7.09	
Pine Sawdust (1.0 – 2.0 mm)	0.25*	4.07	
Pine Sawdust (2.0 – 4.0 mm)	0.28*	3.60	
Corn Stover	0.31	3.21*	Franz (2009)
Dry corn stalks	0.29	3.45*	
Soybean straw	0.24	4.17*	Pelt (2003)
Wet corn stalks	0.24	4.17*	
Dry alfalfa hay	0.23	4.35*	
General	0.28	3.57*	Kaminski (1989)

Note: * estimated from the corresponding value of m or n from sources

By using the information in Table 3, the optimum taper angle can then be determined from the compaction ratios based on the density change of the biomass and the volume change along the screw.

Figure 9(a) shows the plot of the compaction ratio with the taper angle of the screw for different friction coefficients between biomass and barrel, for a screw length of 400 mm, channel depth of 20 mm, helix angle of 17.6° and biomass material coefficient of compressibility of 3.57. It is observed that the taper angle is affected by the friction coefficient at the barrel for a fixed friction coefficient of 0.1 at the screw. A higher friction coefficient at the barrel allows for a higher taper angle. For a friction coefficient of 0.6, the optimum taper angle is observed to be 4.31°, while for friction coefficients of 0.5 and 0.4, the optimum taper angles are 2.95° and 1.83° respectively. The findings are comparable with Zhong (1991) who observed that the taper angle should not be over 3° for a screw five–seven turns long. He noted that if the screw is relatively long and the taper angle is too big, then the material would have difficulties moving forward. From the results presented in Figure 9(a), it can be observed that for taper angle less than the optimum, the biomass material can be compacted conveniently within the channel space but as the taper angle increases beyond the optimum, the reduction of the channel dimensions become greater than the compaction of the biomass material which hinders the positive flow of biomass within the barrel. The compaction ratio is between 1.8 and 3.7 within the acceptable limits of optimum taper angle.

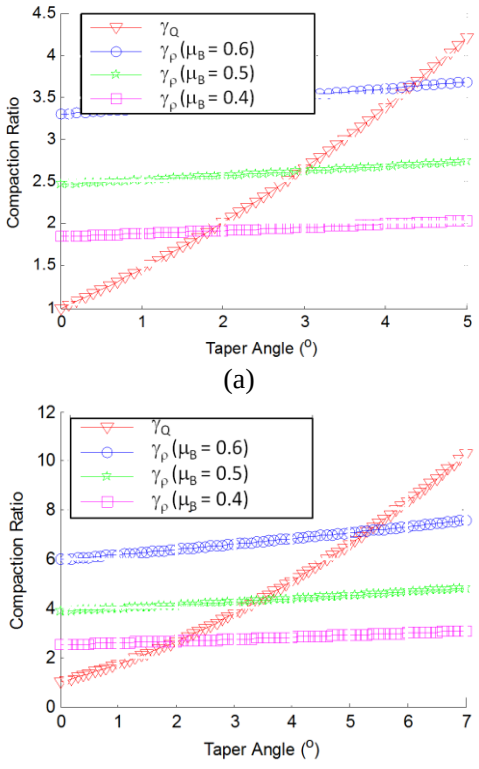

(a)

(b)

Figure 9 Plot of compaction ratio with taper angle for a screw extruder with biomass material with coefficient of compressibility of 3.57 and length of (a) 400 mm and (b) 600 mm

From Figure 9(b), it is seen that a longer screw length can admit a higher taper angle and produce a greater compaction ratio. It is observed that for a screw length of 600 mm, the optimum taper angle for barrel friction coefficient of 0.6 is 5.32°, and for barrel friction coefficients of 0.5 and 0.4, the optimum taper angles are 3.42° and 2° respectively. However, a limiting factor will be the actual compaction ratio of biomass materials. The compaction ratio of screw presses range between 2.5 to 6 or even more. For rice husk, Hood (2010) stated that the compaction ratio was 7.01. Li and Liu (2000) found that, at 138 MPa, the average compaction ratio was about six-eight for mulches, four-five for oak chips and three-four for sawdust. Therefore, limiting the compaction ratio to 5, the optimum taper angle will be less than 4°. This is also comparable with observation of Zhong (1991).

Figure 10 shows the plots of the compaction ratio with taper angle considering different coefficients of compressibility. As discussed earlier, it is unlikely that biomass materials occur as fine materials which, from Table 3, have been shown to have a high coefficient of compressibility. The ideal coefficient of compressibility of biomass material with uniformly distributed particle sizes should range between 3.21 and 4.35 with the average value of 3.57 according to Kaminski (1989) and Pelt (2003). For this range of values, for a screw length of 400 mm, it is observed that the optimum taper angle ranges between 2.27° and 3.4°. The range is seen to be in consistent with the previous recommendation of 3° by Zhong (1991).

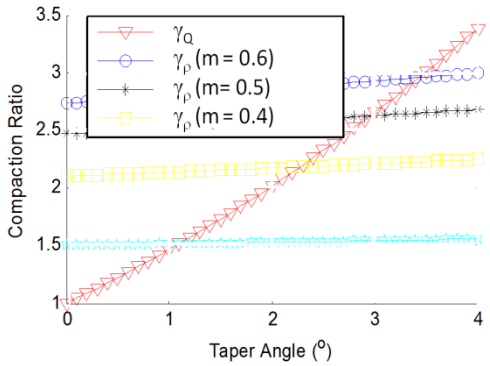

Figure 10 Plot of compaction ratio with taper angle for a screw extruder with biomass materials with different coefficients of compressibility

4 Conclusion

The analysis of the straight screw appears to be complex as contained in existing literatures based on the force and torque balance. The tapered screw is considered to be an effective option for biomass compaction. However, the screw taper introduces greater complications because the geometry is constantly changing. In this study, a method based on the traction and retardation mechanism of friction was developed for a fully unwound screw channel utilizing only the force balances. The procedure has been used to carry out a parametric analysis of the tapered screw extruder for a screw press biomass briquetting machine. The taper angle was considered to significantly increase the pressure developed in the extruder depending on the length of the compaction zone. The optimum taper angle has also been found to be dependent on the frictional coefficient of the biomass material with enclosing surfaces and ranges between 2° and 4° varying with the properties of different biomass materials. The limiting constraint on the choice of optimum taper angle is the actual compaction ratio of the biomass material.

Notation

A	surface area of flow
A	constant regulating form of compressibility function
b	axial distance between flights
B	coefficient of compressibility
$c\_1, c\_2, \ldots c\_31$	constants in compaction equations
D	screw flight diameter
D_1	diameter at screw entry
D_2	diameter at the screw exit
D_B	internal diameter of barrel
D_s	root diameter of the screw
dz	thickness of elemental slice of plug
e	flight thickness
$F1, F2, \ldots, F10$	forces acting on elemental slice of plug
h	screw channel depth
$\bar{h}$	average height of flow, or plug, element
h_z	channel depth along the length of the channel
k	power law coefficient
K	stiffness of particles
L_s	axial length of screw
m	compressibility of material
$\dot{m}$	mass flow rate
N	screw speed
n	power law index
P	pressure
P_{max}	maximum pressure at the end of compaction zone
P_o	initial pressure beneath the hopper
P_x, P_y, P_z	pressure in the respective cartesian directions
Q	volumetric flow rate
V	volume of compact at a specified pressure
V_b	velocity of plug at the barrel
V_{b1}	velocity of screw at the barrel surface
V_{bp}	velocity of plug relative to the barrel
V_p	velocity of plug along the channel
V_{ps}	velocity of plug along the axial length of screw
V_{pz}	velocity of plug parallel to unwound screw root
V_s	void free solid material volume
w	screw channel width
Z	distance along the channel of screw
Z_S	distance along the axial length of screw
α	solids conveying angle
β	channel aspect ratio
γ_Q	compaction ratio based on volume change of the screw
γ_ρ	compaction ratio based on density change in screw
δ	clearance between screw and barrel
θ	taper angle of the channel
ϑ	taper angle of the screw and barrel
κ	stress transmission coefficient
λ	screw pitch
μ_*	overall friction coefficient
μ_B	friction coefficient between plug and barrel
μ_f	friction coefficient between plug and screw flight
μ_S	friction coefficient between plug and screw root
ρ	packing density of compact
ρ_1, ρ_2	particle density of component of a mixture
ρ_f	packing fraction or relative density of material
ρ_{max}	maximum density of material
ρ_o	bulk density of material before compaction
σ	applied stress or pressure
σ_o	initial pressure or stress
ϕ	helix angle
ψ_e	effective angle of powder friction

References

Adapa, P., L. Tabil, and G. Schoenau. 2009. Compression characteristics of selected ground agricultural biomass. *Agricultural Engineering International: the CIGR Ejournal*, Manuscript 1347, Vol. XI, June 2009.

Agur, E. E. 1982. Numerical simulation of a single screw plasticating extruder, PhD Thesis, McMaster University.

Apruzzese, F. 1998. Modelling in extrusion cooking of breakfast cereals, Master of Applied Science Thesis, Department of Chemical Engineering and Applied Chemistry, University of Toronto.

Bilanski, W. K., V. A. Graham, and J. A. Hanusiak. 1985. Mechanics of bulk forage deformation with application to wafering. *Transactions of American Society of Agricultural Engineers*, 28(3): 697-702.

Broyer, E., and Z. Tadmor. 1972. Solids conveying in screw extruders, Part I: A modified isothermal model, Polymer Engineering Science, 12, p. 12.

Campbell, G. A., and N. Dontula. 1995. Solids transport in extruders, International Polymer Proceedings, 10, p.3.

Cooper, A. R., and L. E. Eaton. 1962. Compaction behaviour of several ceramic powders. *Journal of the American Ceramic Society*, 45(3): 97-101.

Darnell, W. H., and E. A. J. Mol. 1956. Solids conveying in extruders. *SPE Journal*, 12(4): 20-29.

Ennis, B. J., W. Witt, D. Sphar, E. Gommeran, R. H. Snow, G. J. Raymus, and J. D. Litster. 2008. Solid-solid operations and processing, Section 21, In Perry's Chemical Engineering Handbook, 8th edition, McGraw-Hill Companies, USA.

Faborode, M. O., and J. R. O'Callaghan. 1986. Theoretical analysis of the compression of fibrous agricultural materials. *Journal of Agricultural Engineering Research*, 35(3): 175-191.

Ferrero, A., J. Horabik, and M. Molenda. 1991. Density-pressure relationships in compaction of straw. *Canadian Agricultural Engineering*, 33(1): 107-111.

Franz, R. D. 2009. Corn stover densification using auger compactor, M.Sc. Thesis, Iowa State University, Iowa.

Gabriele, D., S. Curcio, and B. de Cindio. 2001. Optimal design of a single-screw extruder for liquorice candy production: a rheology based approach. *Journal of Food Engineering*, 48 (2001): 33-44.

Hardman, J. S. 2001. Briquetting of rice husk and production of value-added products from rice husk, Progress Report of DFID Project – R7659: Benefits of Improved Rice Husk Combustion Efficiency, pp. 3-6.

Heckel, R. W. 1961. Analysis of powder compaction phenomenon. *Transactions of the Metallurgical Society of AIME*, 221(5): 1001-1008.

Jones, W. D. 1960. Fundamental principles of powder metallurgy, 242-370, Edward Arnold Publishers Ltd., London.

Kaliyan, N., and R. V. Morey. 2009. Constitutive model for densification of corn stover and switch grass. *Biosystems Engineering*, 104(1): 47-63.

Kaminski, T. 1989. Investigation of the feasibility of collection, densification, storage, transportation, and marketing of agricultural biomass, Saskatoon, Saskatchewan: Saskatchewan Research Council.

Kawakita, K., and K. H. Ludde. 1971. Some considerations on powder compression equations, Powder Technology, 4, pp.61-68.

Larsson, S. H. 2010. Kinematic wall friction properties of reed canary grass powder at high and low normal stresses. *Powder Technology*, 198(1):108-113.

Lovegrove, J. G. A., and Williams. 1970. Solids conveying in a single screw extruder. *Journal of Mechanical Engineering Science*, 15(2): 114-122.

Mani, S., L. G. Tabil, and S. Sokhansanj. 2003. An overview of compaction of biomass grinds. *Powder Handling and Processing*, 15(2):160-168.

Matúš, M., P. Križan, M. Kováčová, and J. Beniak. 2014. The influence of size fraction on the compressibility of pine sawdust and the effectiveness criterion for densification. *Acta Polytechnica* ,54(1): 52-58.

Matúš, M., P. Križan, J. Ondruška, and L. Šooš. 2011. Analysis of tool geometry for screw extrusion machines. *Journal of Applied Mathematics*, 6(2): 404-414.

O'Dogherty, M. J., and J. A. Wheeler. 1984. Compression of straw to high densities in closed cylindrical dies. *Journal of Agricultural Engineering Research*, 29(1): 1-72.

Pelt, T. J. V. 2002. Biomass densification, Report for semester project during the Fall of 2001 for Agricultural Engineering 537 – Crop harvesting dynamics, Iowa State University.

Pelt, T. V. 2003. Maize, soybean and alfalfa biomass densification. *Agricultural Engineering International: the GIGR Journal of Scientific Research and Development*: Manuscript EE 03 002.

Rauwendaal, C. 2004. Extrusion, In Encyclopedia of Polymer Science and Technology, Vol.2, John Wiley & Sons, pp. 497-558.

Schneider, K. 1969. Technical report on plastic processing in the feeding zone of an extruder, Institute of plastics processing, IKV, TH. Aachen.

Sitkei, G. 1986. Mechanics of agricultural materials, Elsevier, Amsterdam.

Sonnergaard, J. M. 2001. Investigation of a new mathematical model for compression of pharmaceutical powders. *European Journal of Pharmaceutical Sciences*, 14(2): 149-157.

Tabil, L. G., and S. Sokhansanj. 1996. Compression and compaction behaviour of alfalfa grinds, Part 1: Compression behaviour. *Powder handling and processing*, 8(1):17-23.

Tadmor, Z., and I. Klein. 1970. Engineering principles of plasticating extrusion, Van Nostrad Reinhold, London.

Tumuluru, J. S., C. T. Wright, K. L. Kenny, and J. R. Hess. 2010a. A review on biomass densification technologies for energy application, Idaho National Laboratory, U.S. Department of Energy, IN/EXT-10-18420, August 2010.

Viswanathan, R., and L. Gothandapani. 1999. Pressure density relationships and stress relaxation characteristics of coir pith. *Journal of Agricultural Engineering Research*, 73(3): 217-225.

Walker, E. E. 1923. The properties of powders-part VI: The compressibility of powders. *Transactions of the Faraday Society*, 19(July): 73-82.

Weert, X., C. J. Lawrence, M. J. Adams, and B. J. Briscoe. 2001. Screw extrusion of food powders: prediction and performance. *Chemical Engineering Science*, 56 (2001): 1933-1949.

Zhong, Z. 1991. Theoretical and experimental analysis of the compaction process in a tapered screw press. Doctor of Philosophy thesis, The University of Newcastle upon Tyne.